Dual-Domain Structural Interference Detection in FDMA based Satellite Communication Networks using Carrier-Aware Spectral Cursor

Sahal Mohammed M N, Abhiram N, Bhimeswara Rao M, Rath D N and Shivani K L
ISRO Telemetry Tracking and Command Network (ISTRAC)
Bangalore, India
e-mail: {sahal | bhimeswar_rao | rathdn | shivani}@istrac.gov.in
{abrm1896}@gmail.com

***Abstract*—Reliable operation of satellite communication links operating in the Frequency Division Multiple Access (FDMA) architecture requires accurate detection of spectral anomalies that may indicate interference, link outage, or carrier distortion. In dense multi-carrier environments, precise identification of interference is essential to avoid misclassifying legitimate carrier energy as anomalous behavior. Conventional automated approaches often apply uniform statistical thresholding across the entire band, making it difficult to distinguish structured carrier energy from genuine interference in heterogeneous spectral conditions. This results in either missed detections within carrier interiors or excessive false alarms near transition regions. This paper proposes a structured dual-domain interference detection framework based on explicit carrier segmentation. A hierarchical carrier-to-noise transition localization strategy with adaptive noise floor estimation first partitions the spectrum into carrier, shoulder, and transition regions. Based on this segmentation, the framework introduces two complementary analytical modules. The Carrier-Aware Spectral Cursor (CASC) is a noise-domain evaluation technique that operates within carrier-adjacent shoulder regions to detect noise floor elevation and transition anomalies. The Carrier Anomaly Detection (CAD) module is a carrier-domain structural analysis method that evaluates internal carrier symmetry and localized envelope deviations to identify distortion or intrusion. By separating noise-domain and carrier-domain logic, the proposed architecture provides a deterministic and interpretable solution for automated interference detection in multi-carrier satellite communication networks. The framework has been deployed within the ISTRAC satellite communication network, operating across geographically distributed ground stations interconnected through FDMA-SCPC architecture.**

Keywords- Satellite Communications; FDMA-SCPC Systems; Interference Detection; Carrier-Aware Spectral Cursor; Carrier Anomaly Detection.

I. INTRODUCTION

Modern satellite communication systems operate in tightly regulated and increasingly congested radio frequency environments, where maintaining spectral integrity is essential for reliable data transfer [1]. In FDMA based Single-Channel-Per-Carrier (SCPC) configurations, multiple geographically distributed ground stations share common satellite transponders within limited bandwidth [2][3].

Under nominal conditions, transponder spectra remain structurally stable and predictable. In operational environments, however, spectral deviations arise due to noise floor elevation, equipment nonlinearity, unintended emissions, or external interference [4]. If not detected in time, these anomalies degrade link margins, weaken carrier isolation, and affect overall communication reliability. Automated and robust interference detection therefore becomes essential in dense multi-carrier deployments.

The challenge is amplified in FDMA-SCPC systems, where carriers differ in bandwidth, modulation, and roll-off characteristics while operating in close spectral proximity. Legitimate carrier energy coexists with noise transitions and measurement artifacts, making interference difficult to distinguish from normal spectral variation. Subtle distortions such as intra-carrier asymmetry, localized intrusion, or gradual noise rise may not produce significant power changes yet can still impair link performance.

Traditional satellite interference monitoring has largely relied on manual spectrum inspection, fixed threshold alarms, and periodic snapshots. Early automated approaches employed power spectral density estimation and statistical energy-based thresholding techniques [5], while more recent studies explored machine learning-assisted spectrum prediction and interference detection [6]. However, multi-carrier spectra are not statistically uniform. Carrier regions exhibit structured high-energy behavior, whereas adjacent noise regions are stochastic. Uniform thresholding often produces false alarms near carrier edges and missed detections within carrier interiors. Although machine learning approaches improve sensitivity, they typically require representative training data and may lack deterministic interpretability in operational satellite systems.

To address these limitations, a structured dual-domain interference detection framework is proposed. The spectrum is first segmented into carrier and noise regions, after which carrier-domain structural assessment is performed independently from noise-domain evaluation. This separation enables consistent detection of both noise-driven and structure-driven interference while preserving interpretability in dense multi-carrier satellite transponders.

The remainder of this paper is organized as follows. Section II presents the proposed dual-domain interference detection methodology, including spectral segmentation, CASC noise-domain analysis, and CAD carrier-domain analysis. Section III discusses the experimental evaluation and detection results obtained from operational satellite transponder spectra. Finally, Section IV concludes the paper and outlines possible future extensions of the proposed framework.

Courtesy of IARIA Board and IARIA Press. Original source: ThinkMind Digital Library https://www.thinkmind.org

II. METHODOLOGY

The proposed methodology establishes a structured dual-domain analytical framework for deterministic interference detection in multi-carrier satellite transponder spectra by combining carrier-aware segmentation, adaptive noise-domain evaluation, and carrier-domain structural analysis.

A. System Architecture Overview

The proposed framework employs a structured dual-domain architecture for automated interference detection. Rather than treating the spectrum as a homogeneous signal field, the method explicitly separates noise and transition regions from verified carrier regions, reflecting practical RF diagnostic reasoning where noise behavior and carrier structure are interpreted independently, as illustrated in Figure 1.

Following spectral acquisition, structured segmentation establishes carrier boundaries and transition zones. Carrier center frequencies are assumed known from the operational frequency allocation plan and serve as initialization anchors for directed transition localization. Domain-specific processing is then applied within each region through the dual-path workflow shown in Figure 2, where noise-domain analysis performs adaptive baseline estimation and detection of unauthorized energy, while carrier-domain analysis evaluates internal envelope symmetry and localized structural deviations.

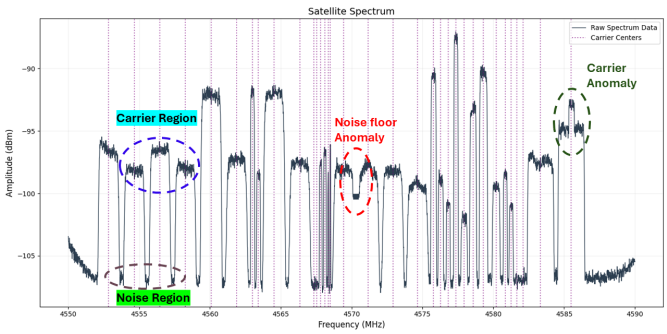

Figure 1. Typical multi-carrier satellite transponder spectrum illustrating carrier regions, noise regions, and representative noise-floor and carrier-structure anomalies.

The outputs of both domains are integrated within a unified decision stage, producing a coherent and interpretable assessment of transponder condition.

B. Data Acquisition and Pre-Processing

The entire acquisition and signal processing workflow is implemented in `Python`, leveraging `PyVISA` for remote instrument control [7] and `NumPy/SciPy` for numerical analysis [8][9]. Spectral measurements are acquired from a `Rohde & Schwarz` spectrum analyzer [10] configured for satellite transponder downlink observation. Fixed measurement parameters, including center frequency, frequency span, resolution bandwidth (RBW), and sweep resolution, are maintained to ensure repeatable and consistent acquisitions across

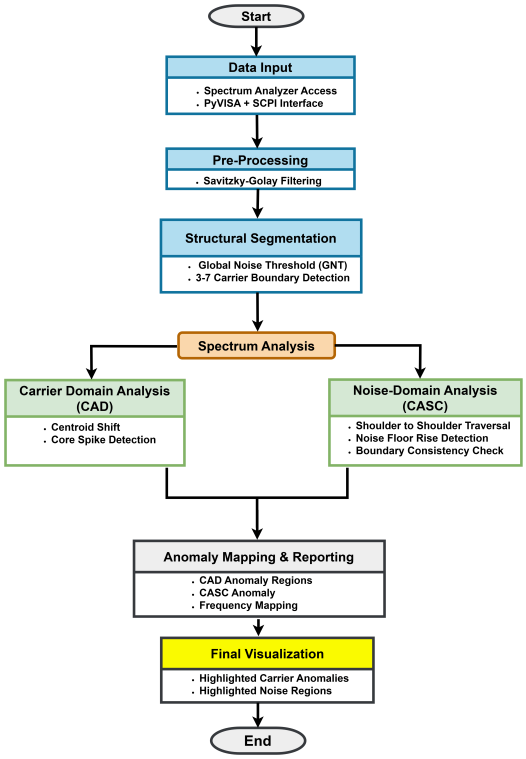

Figure 2. Proposed dual-domain structural interference detection framework with segmentation-driven CASC and CAD processing paths.

monitoring intervals. Each sweep returns a discrete amplitude vector expressed in dBm over the configured transponder bandwidth.

Let the acquired spectrum be represented as in (1)

$$A(f_k), \quad k = 1, 2, \ldots, N \tag{1}$$

where f_k denotes the discrete frequency bins and N is the total number of samples across the observed span.

*1) **Savitzky–Golay Based Smoothing**:* Prior to structural analysis, the measured spectrum undergoes controlled preprocessing to suppress high-frequency measurement noise while preserving carrier envelope geometry. A Savitzky–Golay filter [11] with polynomial order $p = 3$ and window length $2M + 1 = 31$ ($M = 15$) is applied to suppress measurement noise while preserving carrier envelope geometry and transition sharpness.

For each central bin k, the filtered amplitude $\tilde{A}(f_k)$ is obtained by solving the local least-squares problem in (2), where $c_0, c_1, \ldots, c_p$ are the polynomial regression coefficients estimated through local least-squares fitting within the sliding window, and p denotes the polynomial order of the Savitzky–Golay approximation.

$$\min_{c_0, c_1, \ldots, c_p} \sum_{i=-M}^{M} \left[A(f_{k+i}) - \sum_{m=0}^{p} c_m i^m \right]^2 \tag{2}$$

The smoothed value at the window center is given by (3).

$$\tilde{A}(f_k) = c_0 \tag{3}$$

Courtesy of IARIA Board and IARIA Press. Original source: ThinkMind Digital Library https://www.thinkmind.org

This formulation performs local polynomial regression rather than simple averaging, thereby suppressing random spectral fluctuations while preserving carrier peak amplitudes and transition sharpness at carrier boundaries.

The resulting smoothed spectrum $\tilde{A}(f_k)$ is subsequently used for adaptive noise floor estimation, carrier-to noise transition localization, and domain-specific interference detection. This preprocessing stage enhances the stability of threshold-based logic while retaining sensitivity to localized structural distortions within multi-carrier transponder spectra.

C. Structural Spectrum Segmentation

Prior to domain-specific analysis, the spectrum undergoes structural segmentation to establish an adaptive noise reference and to localize carrier-noise separation. These two operations define the analytical framework within which subsequent processing is performed.

Global Noise Threshold (GNT): Adaptive noise floor estimation is performed using a valley-driven sampling strategy. Local minima are identified from a smoothed representation of the spectrum using prominence-based peak detection applied to the inverted trace. For each detected valley index v_i, a neighborhood window of fixed width is sampled to collect representative noise measurements.

Let $\mathcal{N}_i$ denote the set of amplitude samples in the vicinity of the i-th valley. The GNT is defined as the median of the aggregated valley samples shown in (4):

$$GNT = \text{median}\left(\bigcup_i \mathcal{N}_i\right). \quad (4)$$

The median operator provides robustness against sporadic spikes and localized interference. This threshold serves as the reference baseline for noise-domain anomaly detection.

Carrier-to-Noise Transition Localization via Hierarchical 3–7 Trend Analysis: Carrier-to-noise transition localization is performed through directed searches initiated from each carrier center toward both the left and right sides of the spectrum. The objective is to identify structurally stable transition inflection regions where carrier energy consistently decays into the surrounding noise floor. In theory, inflection points correspond to locations where the spectral slope approaches zero. However, direct gradient-based transition detection was found to be unreliable in heterogeneous transponders containing both narrow-band and wide-band carriers. Wide carriers exhibit gradual spectral slopes, resulting in weak or ambiguous first-derivative responses. To ensure robust transition localization, a hierarchical multi-point trend validation strategy is employed. The selected 3-point and 7-point trend evaluations were determined based on the acquisition resolution used throughout the experiments (5000 sweep points over a 40 MHz span, corresponding to approximately 8 kHz per sample). Empirical observation showed that these comparison lengths provided stable transition tracking across varying carrier roll-off conditions, while larger trend windows frequently extended beyond the carrier-to-noise transition region and prematurely reached the noise floor. In addition, the minimum operational carrier data rate considered during evaluation was 64 kbps. Since a 7-point observation window corresponds to approximately 56 kHz of spectral span, the trend validation remained confined within the expected transition behavior of even the narrowest operational carriers while still providing sufficient structural continuity for reliable boundary confirmation.

Initial transition qualification is triggered when the amplitude falls 2 dB below the carrier peak level, establishing a provisional containment threshold. The provisional 2 dB transition criterion was selected empirically to maintain consistency with the minimum carrier qualification condition used by the segmentation stage. Lower thresholds increased sensitivity to noise-floor fluctuations, while higher thresholds reduced boundary sensitivity for low-power carriers. Then, for each candidate index i, local monotonicity trends are evaluated using forward differences as defined in (5):

$$\Delta\tilde{A}_k = \tilde{A}(f_{i+k}) - \tilde{A}(f_{i+k-1}), \quad k = 1, 2, \ldots, N \quad (5)$$

where negative $\Delta\tilde{A}_k$ values indicate downward transitions toward the noise floor.

The detection logic proceeds as follows:

- A 3-point comparison is first applied to verify immediate downward transition consistency.
- If the 3-point validation fails, a 7-point comparison is evaluated to detect broader downward trends.
- If both checks are inconclusive, a fallback trend evaluation is performed using up to 10 consecutive points, requiring at least 75% consistency in downward slope direction.

The 75% consistency requirement was selected empirically to preserve dominant downward trend behavior without enforcing strict monotonic decay. Lower values increased sensitivity to spectral fluctuations, while higher values produced overly restrictive edge validation for closely spaced or gradual roll-off carriers. Once validated, the corresponding index is locked as the carrier-to-noise transition anchor.

D. Noise-Domain Analysis: Carrier Aware Spectral Cursor (CASC)

The Carrier Aware Spectral Cursor (CASC) operates exclusively within the noise and transition regions defined by the structural segmentation stage. Unlike global threshold detectors, CASC is explicitly aware of carrier shoulders and boundary indices derived from the 3–7 trend analysis. This awareness ensures that legitimate carrier energy is excluded from noise-domain evaluation.

1) Shoulder-Constrained Traversal

The CASC engine performs directed traversal between adjacent carriers, analyzing the spectral span from the right shoulder of one carrier to the left shoulder of the next. By confining evaluation to shoulder-to-shoulder regions, the algorithm isolates pure noise intervals while avoiding contamination from carrier interiors.

Courtesy of IARIA Board and IARIA Press. Original source: ThinkMind Digital Library https://www.thinkmind.org

2) Noise Floor Anomaly Detection

Within each shoulder-constrained interval, instantaneous amplitude values are compared against the previously computed GNT. A noise anomaly is declared when the amplitude exceeds the adaptive threshold by a predefined margin. A 1.5 dB margin above the GNT was selected empirically to provide stable separation between normal real-time noise-floor fluctuations and significant spectral anomalies while avoiding excessive sensitivity to transient ripple variations.

Region-growing logic is applied to determine the start and end frequencies of the detected anomaly, ensuring continuous abnormal spans are grouped into a single event. Region growth is initiated when the spectral amplitude exceeds the anomaly declaration margin above the Global Noise Threshold (GNT). The detected span is then expanded across consecutive samples while the amplitude remains above the GNT and outside verified carrier regions. Growth terminates once the spectrum returns to the baseline noise regime or intersects a carrier exclusion boundary.

3) Structural Consistency Verification

In addition to noise elevation detection, CASC evaluates the structural validity of carrier-to-noise transition anchors identified by the 3–7 trend analysis. Specifically, the algorithm checks for abnormal double-rise or double-fall behavior in the vicinity of boundary indices. Such patterns may indicate falsified edge locking due to localized interference or abrupt spectral distortion.

By combining adaptive noise thresholding with transition-consistency validation, CASC provides robust detection of both distributed noise floor changes and localized transition-region anomalies.

Because carrier cores are explicitly excluded, the module remains confined to the noise domain and avoids misclassification of legitimate carrier power variations.

E. Carrier-Domain Analysis: Carrier Anomaly Detection (CAD)

Once the noise-domain assessment is completed, analysis shifts to carrier regions.

Each carrier is treated as a structured spectral entity defined by geometrically stable reference points. The carrier boundaries are determined using -2 dB transition points relative to the carrier peak. These transition points define the effective energy containment region, referred to as the Analysis Window.

All carrier-domain metrics are computed exclusively within this window.

1) Centroid Displacement

The spectral centroid is computed as a power-weighted mean frequency within the analysis window [12]. Deviation of the centroid from the geometric center provides a quantitative measure of envelope symmetry.

Centroid displacement may indicate:

- Asymmetric distortion
- Partial adjacent channel intrusion
- Compression effects

Within the analysis window bounded by f_L and f_R, let the discrete spectrum be represented as $A(f_k)$, where f_k denotes the frequency bin and $A(f_k)$ its corresponding amplitude. The power-weighted spectral centroid is computed as in (6):

$$f_c = \frac{\sum_{k=L}^{R} f_k \, A(f_k)}{\sum_{k=L}^{R} A(f_k)} \tag{6}$$

Centroid displacement relative to the geometric center f_0 is defined as in (7):

$$\Delta f = f_c - f_0 \tag{7}$$

A carrier anomaly is declared when the centroid displacement exceeds 2% of the carrier analysis-window bandwidth. This relative threshold enables consistent structural sensitivity across carriers with varying occupied bandwidths.

2) Core Deviation Metric

The observed carrier envelope is compared against a smoothed reference envelope. The aggregate deviation between the two provides a quantitative measure of distributed structural deformation within the carrier envelope.

Let $\hat{A}(f_k)$ denote the smooth envelope estimate of the carrier. The Core deviation is defined as the normalized mean absolute deviation as shown in (8) :

$$D_{core} = \frac{1}{N} \sum_{k=L}^{R} \left| A(f_k) - \hat{A}(f_k) \right| \tag{8}$$

where N = R - L + 1. This metric captures flattening, uneven shoulder behavior, and gradual envelope deformation.

3) Localized Spike Detection

Localized narrow-band anomalies within the carrier core are detected by evaluating amplitude deviations relative to the median core level. Residual excursions exceeding a predefined threshold are flagged as structural spikes. Localized spike anomalies are declared when core amplitudes exceed the median carrier-core level by 1.5 dB. This margin was selected through operational observation to reduce sensitivity to minor envelope variations while retaining detection capability for embedded narrow-band distortions. This mechanism enables detection of embedded interference components that may not significantly affect global symmetry metrics such as centroid displacement.

F. Decision Fusion Strategy

The outputs of CASC and CAD are interpreted jointly, but remain analytically independent. Decision logic distinguishes between:

- Noise-domain anomalies
- Carrier-domain structural anomalies
- Concurrent disturbances across both domains

This separation enables a clearer classification of transponder spectrum impairments and reduces ambiguity in root-cause interpretation. While CAD evaluates internal carrier structure, CASC maintains noise-domain integrity and boundary consistency, enabling reliable separation of anomaly types.

Courtesy of IARIA Board and IARIA Press. Original source: ThinkMind Digital Library https://www.thinkmind.org

Rather than producing a single aggregated anomaly score, the system preserves domain-level diagnostics, allowing operators to differentiate between noise elevation, carrier deformation, or combined degradation.

III. Results and Discussion

This section presents the experimental validation of the proposed framework using operational satellite transponder spectra, followed by qualitative and quantitative analysis of the obtained interference detection results.

A. Experimental Setup

The proposed framework was evaluated using live spectrum acquisitions from multiple satellite downlinks at the ISTRAC Mission Control Center (MCC). The captured spectra reflected realistic operational loading conditions with heterogeneous carrier bandwidths and power levels. Measurements were obtained through automated acquisition using a fixed analyzer configuration to ensure repeatability. The monitored transponders contained both narrow-band and wide-band carriers operating under varying spectral occupancy conditions, enabling evaluation across heterogeneous carrier spacing and transition behaviors representative of practical FDMA-SCPC satellite deployments.

TABLE I. Dataset Summary

Transponder	Frequency Band	Carrier Count
1	3965-3983 MHz	32
2	3826-3836 MHz	6
3	4550-4590 MHz	34
4	4670-4710 MHz	17

Detection robustness was assessed by introducing controlled spectral disturbances, including localized noise-floor elevation and narrow-band interference relative to known carrier positions. All experiments were performed using the implemented dual-domain architecture without manual adjustment of detected regions.

Table I summarizes the operational transponders used for evaluation, including the monitored frequency ranges and corresponding carrier counts.

For consistent interpretation, a unified visualization scheme is adopted. The GNT is shown as a horizontal grey dashed line, carrier center frequencies as vertical purple markers, and segmentation transition anchors at detected locations. Noise-domain anomalies identified by CASC are highlighted in orange, while carrier-domain anomalies detected by CAD are indicated in red.

B. Noise-Domain Detection Performance (CASC)

The CASC module demonstrated consistent detection of noise-floor elevation and unauthorized spectral energy within shoulder-to-shoulder noise regions. By restricting traversal strictly between carrier boundaries defined by the 3–7 segmentation stage, the algorithm avoided contamination from carrier interior energy and ensured that only noise-domain behavior was evaluated.

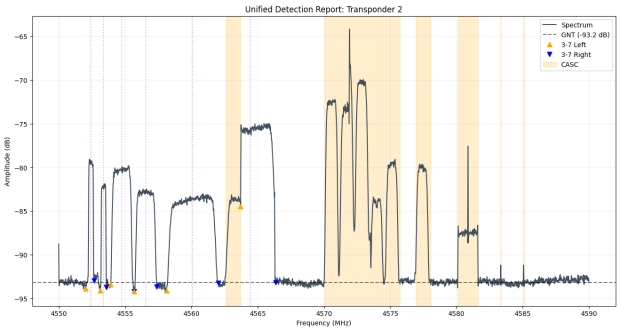

Figure 3. CASC Detection of Transition region and unaware carriers: Transponder 2

Figure 3 illustrates two distinct noise-domain detection scenarios within the same transponder spectrum. The first anomaly, observed near the left-hand side of the central carrier cluster, corresponds to a double-rise transition at a segmented carrier boundary. The boundary consistency validation stage detected this abnormal rise pattern by analyzing directional symmetry around the transition region, thereby preventing incorrect edge locking while preserving accurate carrier boundary localization.

Further toward the right of the same frequency span, multiple spectral structures appear without corresponding carrier segmentation because they are unauthorized transmissions and hence not included in the frequency plan. Since no verified carrier boundaries were established for these signals, CASC treated them as noise-domain intrusions. Using adaptive comparison against the GNT, adjacent abnormal samples were grouped into contiguous detection spans. This enabled reliable identification of previously undefined or unauthorized carriers present within the transponder bandwidth.

C. Carrier-Domain Detection Performance (CAD)

Within verified carrier regions, structural evaluation was performed using centroid-based symmetry analysis and core spike detection.

Centroid displacement effectively captured asymmetric carrier deformation. In cases where spectral energy distribution was skewed toward one side of the carrier bandwidth, the full-window centroid deviated measurably from the core centroid, triggering anomaly flagging. This method proved sensitive to structural leaning without reacting to uniform power scaling.

Core spike detection identified localized narrow-band distortions embedded within otherwise stable carrier envelopes. By comparing core amplitude samples against the median core level, isolated spectral spikes were reliably flagged while maintaining robustness against minor amplitude fluctuations.

Importantly, CAD processing was confined strictly to carrier-defined analysis windows, preventing noise-domain disturbances from influencing carrier structural evaluation.

Courtesy of IARIA Board and IARIA Press. Original source: ThinkMind Digital Library https://www.thinkmind.org

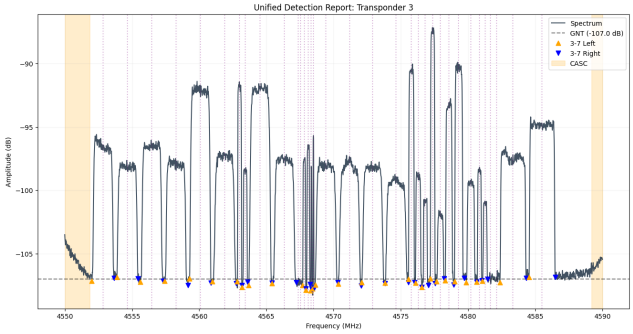

Figure 4. Unified CASC and CAD Detection: Transponder 3- Original

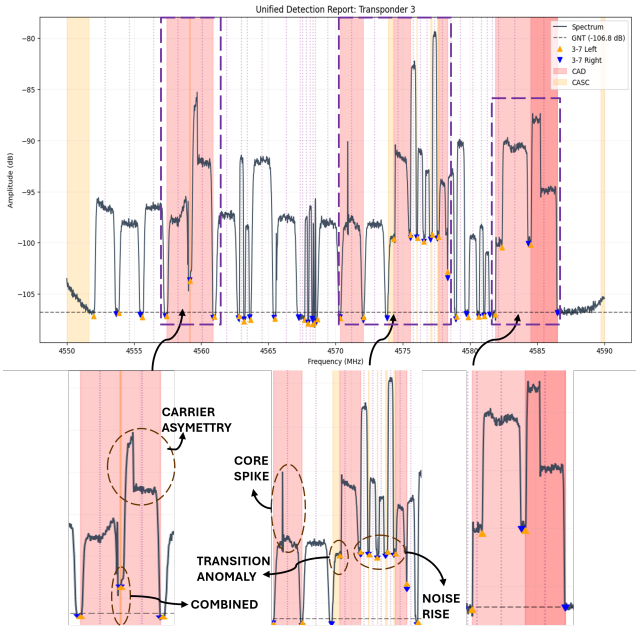

Figure 5. Unified CASC and CAD Detection Results for Transponder 3 with Multiple Injected Noise-Domain and Carrier-Domain Anomalies

D. Joint Diagnostic Interpretation

The separation of noise-domain and carrier-domain analysis provided improved interpretability compared to uniform threshold-based detection approaches. Noise floor rise events were clearly distinguished from carrier-specific structural anomalies, reducing diagnostic ambiguity.

Figure 5 illustrates the controlled interference evaluation performed on Transponder 3, where multiple representative anomaly conditions were intentionally introduced to assess both noise-domain and carrier-domain detection behavior. The highlighted regions demonstrate successful localization of unauthorized spectral activity, transition-region disturbances, carrier asymmetry, and localized structural deformation using the proposed dual-domain framework.

Table II summarizes the controlled interference scenarios evaluated during this experiment together with their corresponding detection modules and outcomes. The results confirm that CASC consistently detected noise-domain and transition-region anomalies, while CAD reliably identified

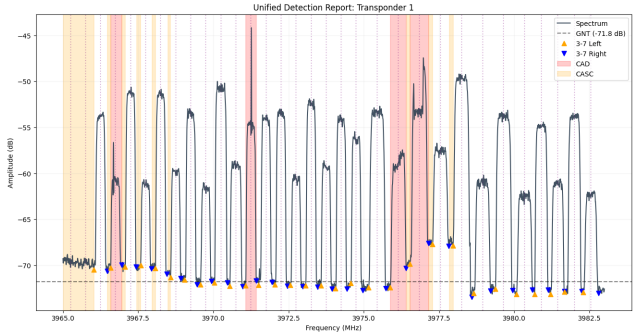

Figure 6. Unified CASC and CAD Detection Results for Transponder 1 with Multiple Noise-Domain and Carrier-Domain Anomalies, Including Nine CASC Detections and Four CAD Structural Detections

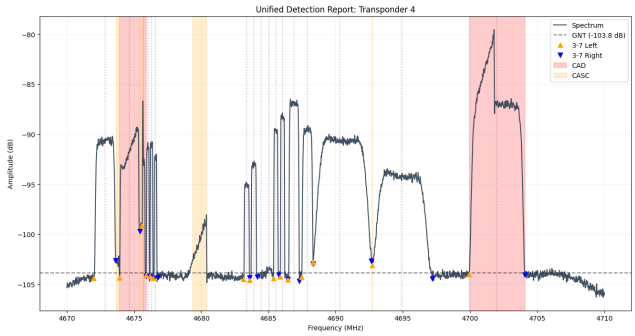

Figure 7. Unified CASC and CAD Detection Results for Transponder 4 Illustrating Unauthorized Carrier and Structural Anomaly Detection

structural carrier distortions and localized intra-carrier abnormalities.

TABLE II. CONTROLLED INTERFERENCE DETECTION SUMMARY

No.	Condition	Module	Result
1	Noise rise	CASC	Detected
2	Unauthorized carrier	CASC	Detected
3	Carrier asymmetry	CAD	Detected
4	Transition anomaly	CASC	Detected
5	Core spike	CAD	Detected
6	Combined distortion	CASC+CAD	Detected

In practical scenarios, this separation enabled differentiation between distributed noise elevation affecting multiple carriers and localized distortion confined to individual carriers. The resulting CAD and CASC reports provided frequency-span localization together with the corresponding anomaly rationale.

The presented results demonstrate that explicit domain separation improves reliability and interpretability in automated transponder spectrum monitoring. Figure 4 shows the nominal transponder spectrum without injected interference, while Figure 5 illustrates combined CASC and CAD detection under injected noise-domain and carrier-domain anomalies. Additional operational spectra in Figures 6 and 7 further validate consistent detection across varying transponder loading conditions, including unauthorized carrier detection by the CASC module in Figure 7.

Courtesy of IARIA Board and IARIA Press. Original source: ThinkMind Digital Library https://www.thinkmind.org

E. Quantitative Performance Evaluation

Quantitative evaluation was performed using known unauthorized carrier injections with predefined ground-truth (GT) frequency spans. The detected anomaly regions obtained from the proposed framework were compared against manually specified start frequency, end frequency, and bandwidth values to evaluate detection accuracy and spectral localization performance. In addition to noise-domain evaluation through CASC, carrier-domain false alarm behavior was assessed using nominal operational carriers monitored across repeated spectrum sweeps.

TABLE III. CASC NOISE-DOMAIN DETECTION PERFORMANCE

Metric	GT 1	GT 2
Start Freq. (MHz)	4626.655	4627.254
End Freq. (MHz)	4626.946	4627.546
Bandwidth	291 kHz	292 kHz
Mean IoU	0.9294	0.9285
Start Error	15.3 kHz	10.3 kHz
End Error	5.6 kHz	11.4 kHz
Bandwidth Error	3.9%	0.4%
P_d	96.1%	99.6%

The CASC module demonstrated consistent detection of unauthorized spectral activity with 96.1% and 99.6% probability of detection across all evaluated sweeps, as summarized in Table III. The high Intersection over Union (IoU) values indicate strong agreement between detected anomaly spans and ground-truth interference regions, while the low start/end frequency errors and bandwidth estimation errors confirm accurate spectral boundary localization performance.

For CAD module, evaluation was performed across nominal operational carriers to assess false alarm behavior under non-anomalous conditions. As shown in Table IV, only 22 false positive detections were observed across 3712 evaluated carriers, resulting in a false alarm probability of 0.5927%. This demonstrates that the proposed structural analysis maintains high sensitivity to carrier deformation while preserving stable operation under normal spectral conditions.

Beyond quantitative accuracy, the proposed framework demonstrated strong operational interpretability during live transponder monitoring. Because CASC and CAD preserve independent domain-level diagnostics, operators can distinguish between distributed noise-floor degradation, unauthorized spectral occupancy, and carrier-specific structural distortion without ambiguity. This separation reduces reliance on manual spectrum inspection and supports faster root-cause assessment in dense FDMA-SCPC satellite environments.

TABLE IV. CAD CARRIER-DOMAIN FALSE ALARM EVALUATION

Metric	Value
Carriers Evaluated	3712
False Positive Flags	22
True Negative Carriers	3690
False Alarm Probability (P_{fa})	0.5927%

IV. CONCLUSION AND FUTURE WORK

This work presented a structured dual-domain framework for automated monitoring of satellite transponder spectra in FDMA-SCPC environments. By introducing explicit carrier segmentation through hierarchical transition localization and adaptive noise floor estimation, the methodology establishes a deterministic structural foundation prior to anomaly evaluation. The separation of noise-domain and carrier-domain processing enables domain-specific detection without statistical cross-contamination. The Carrier-Aware Spectral Cursor (CASC) provides robust surveillance of transition and noise regions, while the Carrier Anomaly Detection (CAD) module evaluates internal carrier symmetry and localized envelope deviations. Their outputs are consolidated within a unified decision framework, preserving interpretability while improving diagnostic clarity.

Unlike uniform global thresholding approaches, the proposed architecture aligns closely with practical RF engineering reasoning and remains fully deterministic and reproducible. The framework has been successfully implemented and evaluated within the ISTRAC satellite communication environment, demonstrating practical applicability in operational multi-carrier FDMA-SCPC systems.

A. Limitations

While the proposed framework provides deterministic and interpretable spectrum monitoring, several limitations remain. Carrier segmentation currently relies on predefined carrier frequency information and fixed threshold margins, which may require retuning under significantly different transponder loading conditions. Since both CASC and CAD depend on accurate structural segmentation, boundary localization inaccuracies may propagate into subsequent domain-specific evaluations and affect anomaly interpretation. In addition, the current implementation remains threshold-driven and does not yet incorporate adaptive learning or statistical optimization mechanisms.

B. Future Work

Future work will focus on adaptive parameter optimization, enhanced structural metrics, and dynamic carrier tracking to improve robustness under highly variable spectral environments. Further development will also include full real-time deployment with integrated GUI-based monitoring for continuous operational surveillance of satellite transponders. Extending the framework toward automated interference localization and operator-assisted anomaly visualization is expected to support smoother SATCOM operations with improved reliability, detection precision, and real-time diagnostic awareness. While the present work focuses on deterministic dual-domain interference detection and operational validation within real satellite transponder environments, future investigations will include comparative performance evaluation against statistical thresholding and machine learning-based interference detection approaches using common benchmark scenarios and controlled spectral injections.

Courtesy of IARIA Board and IARIA Press. Original source: ThinkMind Digital Library https://www.thinkmind.org

ACKNOWLEDGEMENT

The authors acknowledge Dr. A K Anilkumar, Director, ISTRAC and Shri. M R Raghavendra, Associate Director, ISTRAC for encouraging this work. Special appreciation to the SATCOM-ISTRAC team for their valuable feedback during the development and testing phases.

REFERENCES

[1] D. Roddy, *Satellite Communications*, 4th. McGraw-Hill, 2006.

[2] *ITU-R SM.1542: Methods for measurement of spectrum occupancy*, International Telecommunication Union, 2015.

[3] T. Pratt, C. Bostian, and J. Allnutt, *Satellite Communications*, 2nd. Wiley, 2003.

[4] G. Maral and M. Bousquet, *Satellite Communications Systems: Systems, Techniques and Technology*, 5th. Wiley, 2011.

[5] S. M. Kay, *Fundamentals of Statistical Signal Processing: Detection Theory*. Prentice Hall, 1998.

[6] L. Pellaco, N. Singh, and J. Jaldén, "Spectrum prediction and interference detection for satellite communications," *arXiv preprint arXiv:1912.04716*, 2019. DOI: 10.48550/arXiv.1912.04716.

[7] PyVISA Documentation, "Python visa bindings for measurement device control," 2023, [Online]. Available: https://pyvisa.readthedocs.io/ (visited on 05/2026).

[8] C. R. H. et al., "Array programming with numpy," *Nature*, vol. 585, pp. 357–362, 2020. DOI: 10.1038/s41586-020-2649-2.

[9] P. V. et al., "Scipy 1.0: Fundamental algorithms for scientific computing in python," *Nature Methods*, vol. 17, pp. 261–272, 2020. DOI: 10.1038/s41592-019-0686-2.

[10] Rohde & Schwarz, "Spectrum analyzer user manual," Manufacturer Documentation, 2022, [Online]. Available: https://www.rohde-schwarz.com/ (visited on 05/2026).

[11] A. Savitzky and M. J. E. Golay, "Smoothing and differentiation of data by simplified least squares procedures," *Analytical Chemistry*, vol. 36, no. 8, pp. 1627–1639, 1964. DOI: 10.1021/ac60214a047.

[12] A. V. Oppenheim and R. W. Schafer, *Discrete-Time Signal Processing*, 2nd. Prentice Hall, 1999.

Courtesy of IARIA Board and IARIA Press. Original source: ThinkMind Digital Library https://www.thinkmind.org